Microelectronics Journal 39 (2008) 981–991

Microelectronics Journal

www.elsevier.com/locate/mejo

# A comparison of thin film microrefrigerators based on Si/SiGe superlattice and bulk SiGe

Y. Ezzahri*, G. Zeng, K. Fukutani, Z. Bian, A. Shakouri

*Jack Baskin School of Engineering, University of California at Santa Cruz, Santa Cruz, CA 95064-1077, USA*

Received 3 April 2007; received in revised form 22 June 2007; accepted 26 June 2007
Available online 20 August 2007

**Abstract**

Most of the conventional thermal management techniques can be used to cool the whole chip. Since thermal design requirements are mostly driven by the peak temperatures, reducing or eliminating hot spots could alleviate the design requirements for the whole package. Monolithic solid-state microcoolers offer an attractive way to eliminate hot spots. In this paper, we review theoretical and experimental cooling performance of silicon-based microrefrigerators on a chip. Both Si/SiGe superlattice and also bulk SiGe thin film devices have been fabricated and characterized. Direct measurement of the cooling along with material characterization allows us to extract the key factors limiting the performance of these microrefrigerators. Although Si/SiGe superlattice has larger thermoelectric power factor, the maximum cooling of thin film refrigerators based on SiGe alloys are comparable to that of superlattices. This is due to the fact that the superlattice thermal conductivity is larger than bulk SiGe alloy by about 30%.
© 2007 Elsevier Ltd. All rights reserved.

*Keywords:* Microrefrigerator; Si/SiGe superlattices; Bulk SiGe; Heat transfer; Thermoelectric cooling; Thermionic cooling; Thermal quadrupoles method

## 1. Introduction

Thermoelectric coolers are used extensively for temperature stabilization and control of optoelectronic components. Due to an increasing demand for localized cooling and temperature control in the last 10 years, microscale cooling devices have attracted a lot attention for their potential use in hot spot removal in microelectronic and optoelectronic devices, and in some biological applications. Nanostructured materials have manifested very interesting thermoelectric properties, enabling them to have a figure-of-merit $ZT$, exceeding 1 at room temperature. The $ZT$ is defined by $ZT = (\sigma S^2/\beta)T$, where $\sigma$, $S$ and $\beta$ are respectively the electrical conductivity, Seebeck coefficient and thermal conductivity of the thermoelectric material and $T$ is the absolute temperature. SiGe is a known bulk thermoelectric material for high-temperature power generation applications. Recently, Si/SiGe superlattice structures have been investigated for room temperature cooling [1].

Si-based microrefrigerators are attractive for their potential monolithic integration with Si microelectronics. In this paper, we review theoretical and experimental results for silicon-based microrefrigerators on a chip. Both superlattice based on Si/SiGe and also bulk SiGe thin film devices have been fabricated and characterized. Direct measurement of the cooling and cooling power density along with material characterization (e.g. thermal conductivity) allows us to extract the key factors limiting the performance of these microrefrigerators.

In a previous work, Vashaee et al. [2,3] and Zhang et al. [4] proposed a resistive network model to simulate the behavior of microrefrigerators in steady-state regime. In this paper, we use the thermal quadrupoles method (TQM) [5] to describe the microrefrigerators cooling behavior. Prospect for optimization will also be discussed.

The TQM is a general analytical model which predicts electric and thermal responses in a general alternative current (AC) regime, thus making it possible to distinguish, in some cases, the Peltier effect from the Joule effect. In the

*Corresponding author.
*E-mail addresses:* younes@soe.ucsc.edu (Y. Ezzahri), ali@soe.ucsc.edu (A. Shakouri).

0026-2692/$ - see front matter © 2007 Elsevier Ltd. All rights reserved.
doi:10.1016/j.mejo.2007.06.007

case of a pure sine wave electrical excitation, the Peltier effect appears at the same frequency as the operating current, whereas the Joule effect appears at the double frequency. The precision of the TQM allows its application in the detailed characterization of thermoelectric material properties [6]. This method has been used to model the behavior of a conventional thermoelectric couple ($Bi_2Te_3$) [7], and recently the behavior of Si/SiGe microrefrigerators [8,9]. The model presented here uses the limit of the TQM at long times, i.e., steady-state behavior or direct current (DC) regime. Thermophysical properties of the microrefrigerator are assumed to be temperature independent since the absolute cooling is small.

In this model, the different thermal quantities of the microrefrigerator, including the top surface temperature variation and the cooling power density, are calculated by taking into account all possible mechanisms of heat generation and conduction within the entire device. 3D heat and current spreading in the substrate is taken into account. Heat generation in the metal lead connected to the cold top junction and also heat conduction through this lead are also calculated via TQM. All these features make this model more consistent, more complete and closer to real devices than the previous work of Vashaee et al. [2,3] and Ezzahri et al. [8,9].

## 2. Sample description

Fig. 1(a) shows an optical picture of a set of Si-based microrefrigerators with three different sizes. Fig. 1(b) illustrates the schematic cross-sectional view of an Si-based microrefrigerator that we consider in our simulation. A typical composition of the device is as follows [4,10]: it is constituted of an active layer of 3-μm-thick SiGe alloy or Si/SiGe superlattice layer with p-type doping concentration of $5 \times 10^{19}\,cm^{-3}$. The buffer layer is a 1-μm-thick $Si_{0.8}Ge_{0.2}$ film followed by a 1-μm thick $Si_{0.8}Ge_{0.2}/Si_{0.745}Ge_{0.25}C_{0.005}$ superlattice with the same doping concentration as the active layer. The cap layer is 0.3-μm-thick $Si_{0.8}Ge_{0.2}$ film with a doping concentration of $2 \times 10^{20}\,cm^{-3}$ [4]. The most important part of the device is the active SiGe layer. The buffer layer on top of the Si substrate was included in order to reduce the lattice mismatch strain between the substrate and the active layer [11]. The cap layer with the higher doping concentration was included in order to improve the ohmic contact between the metal and the semiconductor. The $SiN_x$ insulating layer is added to prevent any current leaking from the probe into the substrate, thus the current path is confined from the probe to the top of the active SiGe layer before being distributed into the substrate. The Si/SiGe superlattice active layer was grown in a molecular beam epitaxy machine on a 5-in diameter (0 0 1)-oriented Si substrate, and p-type doped to 0.003–0.006 Ωcm with boron. A 1.5–2 μm Ti/Al/Ti/Au layer was evaporated on top of the sample for electrical contact.

## 3. Thermoelectric and thermionic cooling

In an Si-based microrefrigerator, the Peltier cooling occurs at the top metal layer/bulk SiGe or Si/SiGe superlattice junction and also at the buffer layer/substrate junction when the device is fed by a current. The density of heat exchanged with the surrounding medium is characterized by the effective Seebeck coefficient difference at these junctions, and it is proportional to both current intensity and junction temperature [1]. Because of the difference in the Seebeck coefficient values at various interfaces, Peltier cooling or heating is created depending on the direction of the electrical current [1].

In the case where the active layer is a superlattice structure, in addition to thermoelectric cooling, there is a thermionic cooling as it was shown by Shakouri et al. [12,13] and *Mahan* et al. [14], which is an evaporative selective hot electrons filtering effect. Fig. 2(a) shows a cross-sectional transmission electron micrograph of an Si/SiGe thin-film superlattice cooler. Fig. 2(b) shows the energy diagram of a typical thin film superlattice microrefrigerator. These film coolers use the selective emission of hot electrons over a heterostructure barrier layer from the emitter (Cap layer cathode) to the collector (Buffer layer

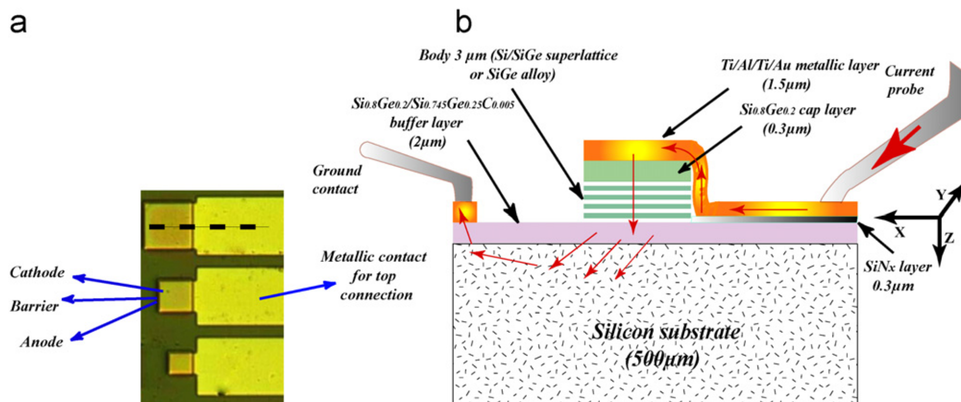


Fig. 1. (a) Optical picture of Si-based microrefrigerators and (b) schematic diagram of the Si-based microrefrigerator cross-sectional view; arrows indicate the direction of electrical current.

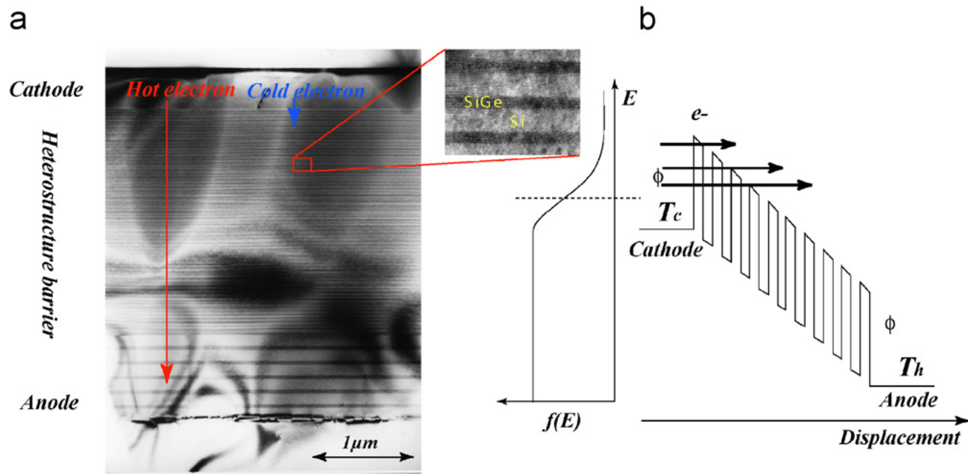


Fig. 2. (a) Transmission electron micrograph of an SiGe thin-film cooler. (b) Schematic energy diagram along with electron energy distribution and Fermi Level (dotted line).

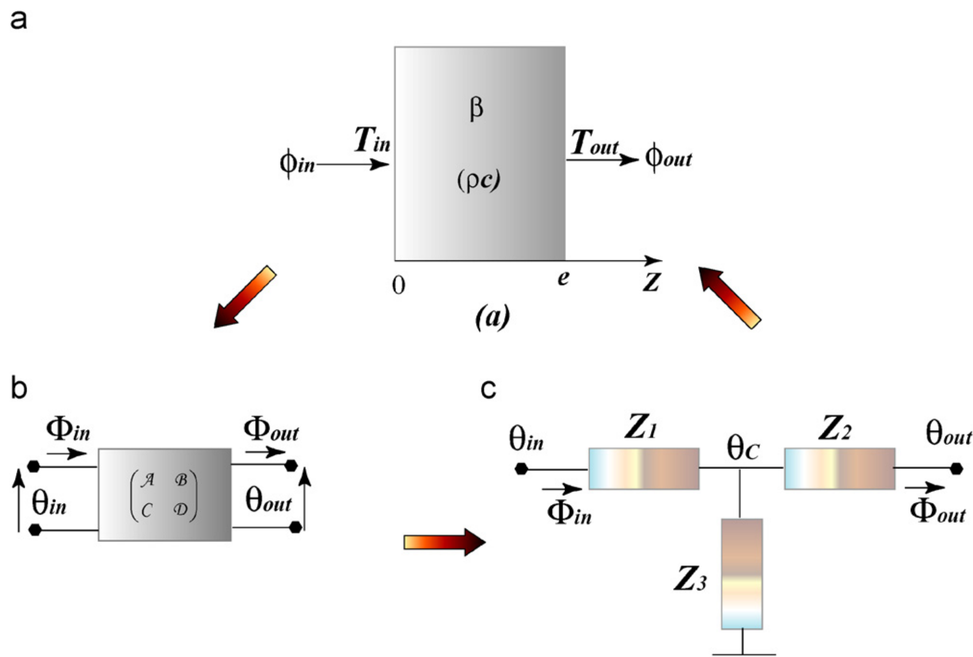


Fig. 3. Thermal quadrupole representation of a passive, linear, homogenous and isotropic layer.

anode) resulting in evaporative cooling. As we can see from Fig. 2(b), since the energy distribution of emitted electrons is almost exclusively on one side of the Fermi energy, upon the current flow, strong carrier–carrier and carrier–lattice scatterings tend to restore the quasi-equilibrium Fermi distribution in the cathode by absorbing energy from the lattice, thus cooling the emitter junction.

Assuming small current densities, we can define an effective Seebeck coefficient for the solid-state thermionic cooling analogous to linear thermoelectric effects. Heating or cooling density at interfaces can then be considered as a linear function of the current [12–15]. In our model, we assume that the effective Seebeck coefficient takes into account both thermoelectric and thermionic phenomena.

## 4. Theoretical model and simulation

Our theoretical model is based on the limit of the TQM at long times. Before starting application of this method to our microrefrigerator, it will be interesting to review in some detail the basis of this method, further details can be found in the original book of Maillet et al. [5].

### 4.1. Basis of the TQM for a passive medium

The TQM is based on the solution of the one-dimensional Fourier's Heat Diffusion Equation (FDHE) in Laplace domain with a zero initial temperature. Fig. 3 illustrates schematically the case of a passive, linear, isotropic and homogenous (PLIH) layer of thickness $e$ in

the general case of the AC regime under adiabatic conditions. The starting point is the following system of equation and its initial boundary condition:

$$\begin{cases} \frac{\partial^2 T}{\partial z^2} - \frac{1 \partial T}{\alpha \partial t} = 0 \quad \text{for } 0 < z < e, \\ T(t=0) = 0 \end{cases} \tag{1}$$

where $\alpha = \beta/(\rho c)$, $\alpha$, $\beta$ and $(\rho c)$ are the thermal diffusivity, thermal conductivity and specific heat per unit volume of the layer, respectively. Let $\theta_{\text{in}}$ and $\theta_{\text{out}}$ be the Laplace transforms of the temperature at $z = 0$ and $e$, respectively, and $\Phi_{\text{in}}$ and $\Phi_{\text{out}}$ be the Laplace transforms of the heat flux at $z = 0$ and $e$, respectively. After Laplace transform, Eq. (1) becomes:

$$\frac{\partial^2 \theta}{\partial z^2} - \frac{p}{\alpha}\theta = 0, \tag{2}$$

where $p$ is Laplace parameter. The solution of this equation is given by

$$\theta(z,p) = C_1 ch(qz) + C_2 sh(qz) \quad \text{with } q^2 = \frac{p}{\alpha}. \tag{3}$$

According to Fourier's heat law, the flux $\phi$ at the abscissa $z$ is associated with the temperature $T$ at the same location by

$$\phi = -\beta\Sigma \frac{\partial T}{\partial z}, \tag{4}$$

where $\Sigma$ is the area of the plane isothermal surface that is considered for the $z$ transfer. After Laplace transform of Eq. (4) and taking into account Eq. (3), we obtain

$$\Phi(z,p) = -\beta\Sigma \frac{\partial \theta}{\partial z} = -\beta\Sigma q[C_1 sh(qz) + C_2 ch(qz)]. \tag{5}$$

The integration constants $C_1$ and $C_2$ can be easily eliminated from Eqs. (3) and (5), written for $z = 0$ and $e$, to provide the following input $(z = 0)$/output $(z = e)$ equations:

$$\begin{cases} \theta_{\text{in}} = ch(qe)\theta_{\text{out}} + \frac{sh(qe)}{K}\Phi_{\text{out}} \\ \Phi_{\text{in}} = K sh(qe)\theta_{\text{out}} + ch(qe)\Phi_{\text{out}} \end{cases} \quad \text{with } K = \beta\Sigma q. \tag{6}$$

The above equations can be written under a matrix form relation relating both vectors $\begin{pmatrix} \theta_{\text{in}} \\ \Phi_{\text{in}} \end{pmatrix}$ and $\begin{pmatrix} \theta_{\text{out}} \\ \Phi_{\text{out}} \end{pmatrix}$ as

$$\begin{pmatrix} \theta_{\text{in}} \\ \Phi_{\text{in}} \end{pmatrix} = \begin{pmatrix} A & B \\ C & D \end{pmatrix} \begin{pmatrix} \theta_{\text{out}} \\ \Phi_{\text{out}} \end{pmatrix} = \begin{pmatrix} ch(qe) & \frac{sh(qe)}{K} \\ K sh(qe) & ch(qe) \end{pmatrix} \begin{pmatrix} \theta_{\text{out}} \\ \Phi_{\text{out}} \end{pmatrix} = M \begin{pmatrix} \theta_{\text{out}} \\ \Phi_{\text{out}} \end{pmatrix}. \tag{7}$$

The particular characteristics of the above matrix ($A = D$ and $Det(M) = 1$) are typical of the transfer matrix of a symmetrical system. Such a system remains unchanged by reversing the propagation $z$-direction, which is similar to the properties of a four terminal electrical network. The later can always be represented by three impedances on either "Π" or "$T$" form scheme. Usually, we prefer "$T$" scheme because it is easier to handle [5]. Such a representation is illustrated in Fig. 3(c). We should note here that the ground level corresponds to the room temperature, the heat flux is the analogous of the electrical current and the temperature is the analogous of the electrical voltage. The impedances are thermal ones and are related to $M$ matrix coefficients by

$$\begin{cases} Z_1 = Z_2 = \frac{A-1}{C}, \\ Z_3 = \frac{1}{C}. \end{cases} \tag{8}$$

Representation by thermal impedances is an analogy to the electrical situation, which corresponds to the relation between the boundary conditions of the layer. The central temperature in Fig. 3(c), i.e. $\theta_C$, does not correspond, anyway, to the temperature at the layer medium. This point has no physical signification. Nevertheless, by replacing $e$ by $(e-z)$ in the matrix $M$ (Eq. (7)), it is possible to know the temperature at every location $z$ within the layer:

$$\begin{pmatrix} \theta_{\text{in}} \\ \Phi_{\text{in}} \end{pmatrix} = \begin{pmatrix} A(e-z) & B(e-z) \\ C(e-z) & D(e-z) \end{pmatrix} \begin{pmatrix} \theta_{\text{out}} \\ \Phi_{\text{out}} \end{pmatrix}. \tag{9}$$

This relation (Eq. (9)) is general whatever the boundary conditions; the only condition is that the heat transfer should be one dimensional.

In the case of a PLIH with lateral losses characterized by a heat convection–radiation coefficient $h$, the matrix relation (Eq. (7)) becomes

$$\begin{pmatrix} \theta_{\text{in}} \\ \Phi_{\text{in}} \end{pmatrix} = \begin{pmatrix} ch(q*e) & \frac{sh(q*e)}{K*} \\ K*sh(q*e) & ch(q*e) \end{pmatrix} \begin{pmatrix} \theta_{\text{out}} \\ \Phi_{\text{out}} \end{pmatrix} \quad \text{with } \begin{cases} q* = \sqrt{\frac{p}{\alpha} + \frac{hm}{\beta\Sigma}}, \\ K* = \beta\Sigma q* \end{cases} \tag{10}$$

where $m$ is the layer perimeter following the two other directions ($x$ and $y$). This relation is the basis of the *thermal fin model* [5], in which a 3D problem can be transformed in a 1D one. If we assume that the heat source is a plane isothermal surface in the $z$-direction, then the thermal fin model can be applied for a small Biot number following the two other lateral directions $Bi = (hL_{x,y}/\beta) < 0.1$ [5], $L_{x,y}$ are the characteristic lengths of the medium in the lateral directions $x$ and $y$. This case is more likely to happen for media of high thermal conductivities and/or low dimensions. In this case, the radial temperature gradient can be neglected with respect to the longitudinal one.

### *4.2. Basis of the TQM for an active medium*

Let us now assume a linear, isotropic and homogeneous layer of thickness $e$ with a delocalized internal heat source as it is illustrated schematically in Fig. 4(a). This source will

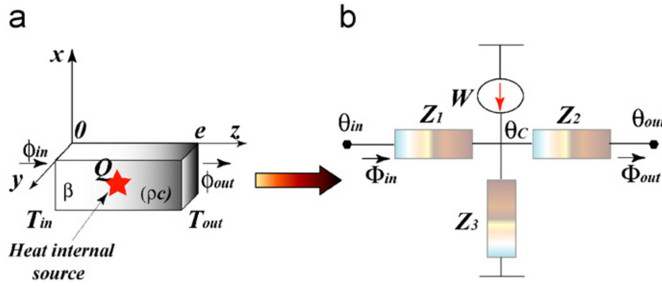


Fig. 4. Thermal quadrupole representation of an active, linear, homogenous and isotropic layer.

be modeled by a thermal current source placed at the central point of the thermal circuit as it is represented in Fig. 4(b). We should note here also that this representation is again a picture of mind, regarding the delocalized character of the internal heat source. The choice is completely independent of the boundary conditions [5].

The matrix relation between the temperature-heat flux vectors is now given by [7,10]

$$\begin{pmatrix} \theta_{\text{in}} \\ \Phi_{\text{in}} \end{pmatrix} = \begin{pmatrix} ch(qe) & \frac{sh(qe)}{K} \\ Ksh(qe) & ch(qe) \end{pmatrix} \begin{pmatrix} \theta_{\text{out}} \\ \Phi_{\text{out}} \end{pmatrix} - \begin{pmatrix} Z_1 W \\ W \end{pmatrix}, \tag{11}$$

where $W$ represents the internal heat source. In our case treated later in the paper, the internal heat source is the Joule heat generation within each layer of the device. In Eq. (11), we have assumed that the lateral heat losses are neglected. We should note here that the punctual representation of $W$ does not make any confusion about its volume character, which is included in its expression [5]:

$$W = \frac{1}{e}\int_0^e Q(z,p)ch(qz)\,\mathrm{d}z, \tag{12}$$

where $Q(z,p)$ is the Laplace transform of the internal heat source. As we can see in Eq. (11), the matrix coefficients are the same like in the case of a passive layer, which means that these coefficients do not depend on the internal source or the initial temperature distribution [5].

### 4.3. TQM in the DC regime

The case of the DC regime can be considered as the limit of the AC regime for very long times, which means that the Fourier number $\alpha t/e^2$ tends to infinity or its equivalent in Laplace domain $e^2p/\alpha$ tends to zero [5]. In this case, Eq. (8) becomes

$$\begin{cases} Z_1 = Z_2 \rightarrow \dfrac{e}{2\beta\Sigma} = \dfrac{R^{\text{the}}}{2} \text{pure thermal resistance,} \\ Z_3 \approx \dfrac{1}{(\rho c)e\Sigma p} = \dfrac{1}{C^{\text{the}}p} \text{pure thermal capacitance.} \end{cases} \tag{13}$$

The matrix relation in the case of the DC regime is then obtained by multiplying each line of Eq. (11) by $p$ and taking the limit when $p$ goes to zero. It follows from the final value theorem for Laplace transform that

$$\begin{aligned} \begin{pmatrix} T_{\text{in}} \\ \phi_{\text{in}} \end{pmatrix} &= \begin{pmatrix} ch(qe) & \frac{sh(qe)}{K} \\ Ksh(qe) & ch(qe) \end{pmatrix}_{\lim_{p\to 0}} \begin{pmatrix} T_{\text{out}} \\ \phi_{\text{out}} \end{pmatrix} \\ &\quad - \begin{pmatrix} Z_1 \\ 1 \end{pmatrix} (p \times W)_{\lim_{p\to 0}} \\ &= \begin{pmatrix} 1 & R^{\text{the}} \\ 0 & 1 \end{pmatrix} \begin{pmatrix} T_{\text{out}} \\ \phi_{\text{out}} \end{pmatrix} - \begin{pmatrix} R^{\text{the}}/2 \\ 1 \end{pmatrix} J \\ &\text{with } J = \lim_{p\to 0}(p \times W). \end{aligned} \tag{14}$$

### 4.4. Application of TQM to the microrefrigerator in the DC regime

The microrefrigerator layers thicknesses are several orders of magnitude larger than the mean free path of both electrons and phonons [16]. We can hence assume a diffusive transport regime, and the FDHE can then be used. When the active layer is a superlattice, because individual layers within it are very thin, on the order of nanometers, the superlattice is considered as an effective medium.

#### 4.4.1. Heat transport in the cross-plan direction of the microrefrigerator

The thickness of the active SiGe layer is very small compared to that of the substrate; moreover, all Peltier sources are uniform at all junction plans. We thus consider the heat transfer across the microrefrigerator to be one-dimensional in the cross-plan direction of the device. We neglect heat transfer at the side surface area around the mesa due to convection and radiation. We assume adiabatic conditions at these surfaces. This can be justified due to the small dimensions of the microrefrigerator and the marginal cooling temperature reduction. Our structure is formed of four essential layers; the heat transfer matrix of each layer can be written in the form

$$\begin{pmatrix} T_{\text{in}} \\ \phi_{\text{in}} \end{pmatrix} = \begin{pmatrix} 1 & R_{\text{i}}^{\text{the}} \\ 0 & 1 \end{pmatrix} \begin{pmatrix} T_{\text{out}} \\ \phi_{\text{out}} \end{pmatrix} - \begin{pmatrix} \frac{R_{\text{i}}^{\text{the}}}{2} \\ 1 \end{pmatrix} J_{\text{i}}. \tag{15}$$

The term $J_i$ indicates the internal Joule heating source inside each layer, and is given by

$$J_{\text{i}} = R_{\text{i}}^{\text{ele}} I_{\text{e}}^2, \tag{16}$$

where $R_i^{\text{ele}}$ and $I_{\text{e}}$ are the electrical resistance of each layer and the amplitude of the excitation current, respectively. The subscript $i = $ m, cl, al, bl stands for the metallic layer, the cap layer, the active SiGe layer and the buffer layer, respectively.

*4.4.2. Heat transport within the substrate*

Regarding the local character of the microrefrigerator, the silicon substrate underneath it is considered thermally thick and its effect will be contained in what is called the *Resistance of constriction or spreading*. Constriction and spreading resistances exist whenever heat flows from one region to another of different cross-sectional area. The term constriction is used to describe the situation where heat flows out from a large cross-sectional region into a narrower one, and the term spreading is used to describe the opposite case where heat flows out of a narrow region into a larger cross-sectional area.

Approximating both the microrefrigerator and the substrate with a cylindrical geometry, the thermal constriction/spreading resistance is given by [5]

$$R_{\mathrm{Sub}}^{\mathrm{the},1}=\frac{8}{3\pi^2\beta_{\mathrm{Sub}}r}\quad\text{with}\quad r=\sqrt{\Sigma/\pi},\tag{17}$$

where $r$ is the radius of the contact disc between the two media, $\Sigma$ is the cross-sectional area of the microrefrigerator and $\beta_{\mathrm{Sub}}$ is thermal conductivity of the substrate.

In fact, the expression of this constriction/spreading resistance depends on the form of temperature and flux distributions in the [0, $r$] interval. Eq. (17) is valid in the case of uniform flux distribution in this interval which should match better the physics. One should note that the difference in the expressions of the constriction/spreading resistances between the case of uniform flux distribution and the case of uniform temperature distribution in the [0, $r$] interval is only 8% [5]. In addition to the thermal spreading inside the substrate, there is an electrical current spreading. Joule heating is mainly localized at the buffer-layer/substrate interface [17]. This electrical spreading is characterized by a spreading of the electrical current density lines in the substrate. Although heat current flow is different from electrical current flow due essentially to the notion of skin effect related to electrical current; however, in the DC regime, this notion has no significance and then the electrical constriction/spreading resistance can be calculated in analogy with the thermal resistance, and is given by the equation:

$$R_{\mathrm{Sub}}^{\mathrm{ele}}=\frac{8}{3\pi^2\sigma_{\mathrm{Sub}}r},\tag{18}$$

where $r$ is the radius of the contact disc between the microrefrigerator and the substrate, and $\sigma_{\mathrm{Sub}}$ is the electrical conductivity of the substrate.

*4.4.3. Heat transport within the top side contact of the microrefrigerator*

The top side metal lead is provided to carry the current to the cold junction, but it turns out that it is responsible for some part of Joule heating, which limits the maximum cooling. The temperature change within this metal lead is dominant in the longitudinal direction ($X$ direction) and, therefore, the metal lead can be viewed as a thermal fin. To describe heat transfer within this metal lead, Wang et al. [18] have solved directly the heat diffusion equation in the longitudinal direction with two appropriate boundary conditions, which are (i) a constant temperature at the interface metal lead/microrefrigerator top surface and (ii) a zero heat flux at the other end of the metal lead. In our analysis, we still use TQM in the longitudinal direction of the metal lead by assuming the same boundary conditions as Wang et al. [18]. The width of the metal lead is supposed to be equal to the side of the microrefrigerator device. As for the microrefrigerator, the top metal lead surface is considered adiabatic, but heat conduction from the bottom surface of the metal lead through the $\mathrm{SiN}_x$ layer and the buffer layer into the silicon substrate is described by an effective heat transfer coefficient given by

$$h_{\mathrm{eff}}=\frac{1}{(R_{\mathrm{SiN}_x}+R_{\mathrm{Buffer}}+R_{\mathrm{Sub}}^{\mathrm{the},2})\,l_{\mathrm{m}}w_{\mathrm{m}}},\tag{19}$$

where $R_{\mathrm{SiN}_x}$, $R_{\mathrm{Buffer}}$ and $R_{\mathrm{Sub}}^{\mathrm{the},2}$ are the thermal resistances of the $\mathrm{SiN}_x$ layer, buffer layer and substrate, respectively.

Due to the low thicknesses of the $\mathrm{SiN}_x$ and the buffer layers in comparison with the substrate, heat conduction inside them is assumed to be one dimensional and perpendicular to the bottom surface of the metal lead. Their corresponding thermal resistances are thus given by

$$\begin{cases}R_{\mathrm{SiN}_x}=\dfrac{t_x}{\beta_x l_x w_x},\\[2mm] R_{\mathrm{Buffer}}=\dfrac{t_{\mathrm{b}}}{\beta_{\mathrm{bl}}l_{\mathrm{bl}}w_{\mathrm{bl}}},\end{cases}\tag{20}$$

where $t_x$, $t_{\mathrm{bl}}$, $\beta_x$ and $\beta_{\mathrm{bl}}$, are the thickness and the thermal conductivity of the $\mathrm{SiN}_x$ layer and the buffer layer, respectively. $l_x=l_{\mathrm{bl}}=l_{\mathrm{m}}$ and $w_x=w_{\mathrm{bl}}=w_{\mathrm{m}}=\sqrt{\Sigma}$ are the length and the width of the metal lead.

As the length of the metal lead is larger than its width, the heat conduction downwards in the silicon substrate is assumed to take the form of two dimensional spreading (in $Y$–$Z$ plane), and the average value of the spreading thermal resistance can be calculated as [18]

$$R_{\mathrm{Sub}}^{\mathrm{the},2}=\frac{1}{2\beta_{\mathrm{Sub}}l_m}\left[\delta+\frac{2}{\pi^3\varepsilon^2}\sum_{n=1}^{\infty}\frac{\sin^2(n\pi\varepsilon)}{n^3}\tanh(n\pi\delta)\right],\tag{21}$$

where $\delta=2t_{\mathrm{sub}}/w_{\mathrm{sub}}$ and $\varepsilon=w_{\mathrm{m}}/w_{\mathrm{sub}}$. $t_{\mathrm{Sub}}$, $w_{\mathrm{Sub}}$ and $\beta_{\mathrm{Sub}}$ are the thickness, width and thermal conductivity of the substrate. One can note here that the substrate underneath the metal lead is considered as a finite medium at the opposite of the microrefrigerator device. This is because of the relatively larger size of the side metal lead.

Application of TQM to the DC heat transfer along the metal lead allows writing the following matrix relation between the temperature–heat flux vectors at both sides of

the metal lead:

$$\begin{pmatrix} T_{\rm in}^{\rm ML} \\ \phi_{\rm in}^{\rm ML} \end{pmatrix} = \begin{pmatrix} {\rm ch}(\sqrt{(h_{\rm eff}/\beta_{\rm m}t_{\rm m})}l_{\rm m}) & {\rm sh}(\sqrt{(h_{\rm eff}/\beta_{\rm m}t_{\rm m})}l_{\rm m})/\beta_{\rm m}w_{\rm m}t_{\rm m}\sqrt{(h_{\rm eff}/\beta_{\rm m}t_{\rm m})} \\ \beta_{\rm m}w_{\rm m}t_{\rm m}\sqrt{h_{\rm eff}/\beta_{\rm m}t_{\rm m}}{\rm sh}(\sqrt{h_{\rm eff}/\beta_{\rm m}t_{\rm m}}l_{\rm m}) & {\rm ch}(\sqrt{(h_{\rm eff}/\beta_{\rm m}t_{\rm m})}l_{\rm m}) \end{pmatrix} \times \begin{pmatrix} T_{\rm out}^{\rm ML} \\ \phi_{\rm out}^{\rm ML} \end{pmatrix} - \begin{pmatrix} Z_1^{\rm ML} \\ 1 \end{pmatrix} J_{\rm ML} \quad (22)$$

where

$$\begin{cases} Z_1^{\rm ML} = \dfrac{{\rm ch}(\sqrt{(h_{\rm eff}/\beta_{\rm m}t_{\rm m})}l_{\rm m}) - 1}{\beta_{\rm m}w_{\rm m}t_{\rm m}\sqrt{h_{\rm eff}/\beta_{\rm m}t_{\rm m}}{\rm sh}(\sqrt{(h_{\rm eff}/\beta_{\rm m}t_{\rm m})}l_{\rm m})}, \\ J_{\rm ML} = R_{\rm ML}^{\rm ele} I_{\rm e}^2 \dfrac{{\rm sh}(\sqrt{(h_{\rm eff}/\beta_{\rm m}t_{\rm m})}l_{\rm m})}{\sqrt{(h_{\rm eff}/\beta_{\rm m}t_{\rm m})}l_{\rm m}}, \\ R_{\rm ML}^{\rm ele} = \dfrac{l_{\rm m}}{\sigma_{\rm m}w_{\rm m}t_{\rm m}}, \end{cases} \quad (23)$$

where $t_{\rm m}$ and $\sigma_{\rm m}$ are the thickness and the electrical conductivity of the metal lead. As we can see in the expression of the Joule heating $J_{\rm ML}$, it contains an additional factor with respect to Eq. (16). In fact, this factor describes heat leakage from the metal lead to the substrate via the effective heat transfer coefficient $h_{\rm eff}$.

The particular characteristics of the above transfer matrix allow representing the metal lead by a set of thermal impedances as shown in Fig. 5(a). Those thermal impedances depend on the corresponding transfer matrix coefficients:

$$\begin{cases} Z_1^{\rm ML} = Z_2^{\rm ML} = \dfrac{ch\left(\sqrt{\dfrac{h_{\rm eff}}{\beta_{\rm m}t_{\rm m}}}l_{\rm m}\right) - 1}{\beta_{\rm m}w_{\rm m}t_{\rm m}\sqrt{\dfrac{h_{\rm eff}}{\beta_{\rm m}t_{\rm m}}}sh\left(\sqrt{\dfrac{h_{\rm eff}}{\beta_{\rm m}t_{\rm m}}}l_{\rm m}\right)}, \\ Z_3^{\rm ML} = \dfrac{1}{\beta_{\rm m}w_{\rm m}t_{\rm m}\sqrt{\dfrac{h_{\rm eff}}{\beta_{\rm m}t_{\rm m}}}sh\left(\sqrt{\dfrac{h_{\rm eff}}{\beta_{\rm m}t_{\rm m}}}l_{\rm m}\right)}. \end{cases} \quad (24)$$

The second boundary condition (zero flux at the beginning of the metal lead) allows us to get the relation between the heat flux at the interface metal lead/ microrefrigerator and the temperature variation at the top surface of the later. In fact, it is easy to see that $\phi_{\rm ML}^{\rm in} = 0$ leads to

$$\phi_{\rm ML}^{\rm out} = \phi_{C1} = R_{\rm ML}^{\rm ele}\sqrt{\frac{\beta_{\rm m}t_{\rm m}}{l_{\rm m}^2 h_{\rm eff}}}th\left(\sqrt{\frac{h_{\rm eff}}{\beta_{\rm m}t_{\rm m}}}l_{\rm m}\right)I_{\rm e}^2 - \sqrt{\beta_{\rm m}t_{\rm m}w_{\rm m}^2 h_{\rm eff}}\,th\left(\sqrt{\frac{h_{\rm eff}}{\beta_{\rm m}t_{\rm m}}}l_{\rm m}\right)T_{C1} \quad (25)$$

$T_{C1}$ represents the temperature variation at the top surface of the microrefrigerator. The first term in Eq. (25) describes Joule heating generation within the metal lead whereas the second term describes heat conduction due to the temperature gradient within it. Both of those effects will reduce the effective cooling rate of the microrefrigerator and thus degrade the cooling performance. We also demonstrated that the ohmic contact resistance $R_{\rm C}^{\rm Ohm}$ between the cap layer and the metallic layer is another important limiting factor on the performance of the microrefrigerator [4].

Figs. 5(a) and (b) illustrate, respectively, the quadrupole system associated with the DC heat transfer inside the metal lead, and the global quadrupole system associated with the DC heat transfer within the entire microrefrigerator device. Application of Kirchhoff laws to this system, allows us to get a matrix relation, which represents the DC heat transfer in the entire structure between $\begin{pmatrix} T_{C1} \\ \phi_{C1} \end{pmatrix}$ and $\begin{pmatrix} T_{C2} \\ \phi_{C2} \end{pmatrix}$, the temperature–heat flux vectors at the top metallic layer and the interface buffer layer/substrate, respectively:

$$\begin{pmatrix} T_{C1} \\ \phi_{C1} \end{pmatrix} = \begin{pmatrix} 1 & R_{\rm m}^{\rm the} + R_{\rm cl}^{\rm the} + R_{\rm al}^{\rm the} + R_{\rm bl}^{\rm the} \\ 0 & 1 \end{pmatrix} \times \begin{pmatrix} T_{C2} \\ \phi_{C2} - P_{\rm BS} - J_{\rm Sub} \end{pmatrix} - \begin{pmatrix} 1 & R_{\rm m}^{\rm the} + R_{\rm cl}^{\rm the} + R_{\rm al}^{\rm the} \\ 0 & 1 \end{pmatrix} \begin{pmatrix} \dfrac{R_{\rm bl}^{\rm the}}{2}J_{\rm bl} \\ J_{\rm bl} \end{pmatrix} - \begin{pmatrix} 1 & R_{\rm m}^{\rm the} + R_{\rm cl}^{\rm the} \\ 0 & 1 \end{pmatrix} \begin{pmatrix} \dfrac{R_{\rm al}^{\rm the}}{2}J_{\rm al} \\ J_{\rm al} \end{pmatrix} - \begin{pmatrix} 1 & R_{\rm m}^{\rm the} \\ 0 & 1 \end{pmatrix} \begin{pmatrix} \dfrac{R_{\rm cl}^{\rm the}}{2}J_{\rm cl} \\ J_{\rm cl} + P_{\rm MC} + J_C^{\rm Ohm} \end{pmatrix} - \begin{pmatrix} \dfrac{R_{\rm m}^{\rm the}}{2}J_{\rm m} \\ J_{\rm m} \end{pmatrix} \quad (26)$$

where

$$\begin{cases} P_{\rm MC} = (S_{\rm M} - S_{\rm AL})I_{\rm e}T_0, P_{BS} = (S_{\rm AL} - S_{\rm Sub})I_{\rm e}T_0 \\ J_{\rm Sub} = R_{\rm Sub}^{\rm ele}I_{\rm e}^2, J_C^{\rm Ohm} = R_C^{\rm Ohm}I_{\rm e}^2 \\ \phi_{C2} = \dfrac{T_{C2}}{R_{\rm Sub}^{\rm the,1}} \end{cases} \quad (27)$$

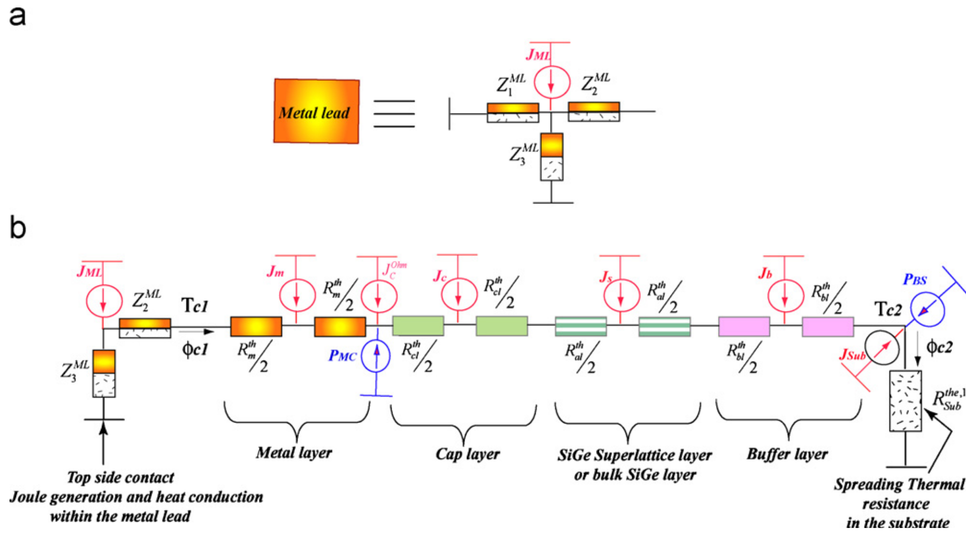


Fig. 5. (a) Thermal quadrupole network associated with the heat transfer within the top side metal lead and (b) thermal quadrupole network associated with the heat transfer within the whole SiGe microrefrigerator in the steady-state regime.

$S_M$, $S_{AL}$, and $S_{Sub}$ are the absolute Seebeck coefficients of the metal layer, active SiGe layer, and substrate, respectively. The effective active layer Seebeck coefficient, $S_{AL}$, include both thermoelectric and thermionic contributions in the case where the active layer is a Si/SiGe superlattice, as we have mentioned above. $T_0$ is the average temperature of the junction. Previous simulations in the general case of the AC regime have shown that for small excitation current amplitudes, linear approximation still possible and approximating the interface temperature with the room temperature still reasonably correct [7,10]. For this reason, in the whole simulation, we keep the average temperature of the junction equal to the room temperature 300 K [7,10].

Combining Eqs. (25–27) allows us to get the expression of the microrefrigerator top surface temperature variation $T_{C1}$ as a function of the excitation current amplitude $I_e$, as well as all physical and geometrical parameters of the whole device. The expression of the $T_{C1}$ is given by

$$T_{C1} = \frac{1}{G_{Tot}} \left\{ \begin{array}{l} (P_{BS} + J_{Sub}) + \left[ 1 + \dfrac{R_{cl}^{the} + R_{al}^{the} + R_{bl}^{the}}{R_{Sub}^{the,1}} \right] (P_{MC} + J_C^{Ohm}) \\ + \left[ 1 + \dfrac{R_m^{the} + R_{cl}^{the} + R_{al}^{the} + R_{bl}^{the}}{R_{Sub}^{the,1}} \right] \\ \left( \Delta + R_{ML}^{ele} \sqrt{\dfrac{\beta_m t_m}{l_m^2 h_{eff}}} th \left( \sqrt{\dfrac{h_{eff}}{\beta_m t_m}} l_m \right) I_e^2 \right) - \dfrac{\Gamma}{R_{Sub}^{the,1}} \end{array} \right\} \tag{28}$$

where $G_{Tot}$, $\Delta$ and $\Gamma$ are defined by

$$\left\{ \begin{array}{l} G_{Tot} = \dfrac{1 + \sqrt{\beta_m t_m w_m^2 h_{eff}}\, th \left( \sqrt{\dfrac{h_{eff}}{\beta_m t_m}} l_m \right) \left[ R_{Sub}^{the,1} + R_m^{the} + R_{cl}^{the} + R_{al}^{the} + R_{bl}^{the} \right]}{R_{Sub}^{the,1}} \\ \Delta = J_{bl} + J_{al} + J_{cl} + J_m \\ \Gamma = \left( \dfrac{R_{bl}^{the}}{2} + R_m^{the} + R_{cl}^{the} + R_{al}^{the} \right) J_{bl} + \left( \dfrac{R_{al}^{the}}{2} + R_m^{the} + R_{cl}^{the} \right) J_{al} + \left( \dfrac{R_{cl}^{the}}{2} + R_m^{the} \right) J_{cl} + \dfrac{R_m^{the}}{2} J_m \end{array} \right. . \tag{29}$$

## 5. Results and discussion

The cooling performance was measured using standard type E microthermocouple with a tip size of 50 μm. The ILX Lightwave LDX3220 current source was used to supply a stable current to the microrefrigerator through probes. The microthermocouple tips were placed on top of the sample and the substrate. HP 34420A Nanovoltage/microOhm meter was used to measure the voltage difference between the two microthermocouple tips. A Labview® program was developed to automatically control measurements and convert the voltage difference to temperature using temperature calibration data offered by the manufacturer. A schematic diagram of the experimental setup is illustrated in Fig. 6. Fig. 7 shows the experimental cooling versus current data for thin film bulk SiGe (a) and Si/SiGe superlattice (b) for different device sizes.

As we can see in Fig. 8, both microrefrigerators with bulk SiGe and Si/SiGe superlattice produce almost the same cooling for each device size. Although separate 3ω measurements [19] have shown that bulk SiGe alloy has a thermal conductivity which is about 30% lower than that of Si/SiGe superlattice, the later compensate this difference in the power factor as we can see in Table 1. This table recapitulates material parameters of bulk SiGe alloy and Si/SiGe superlattice measured and estimated at room temperature for a $60 \times 60\,\mu m^2$ device size. Due to the

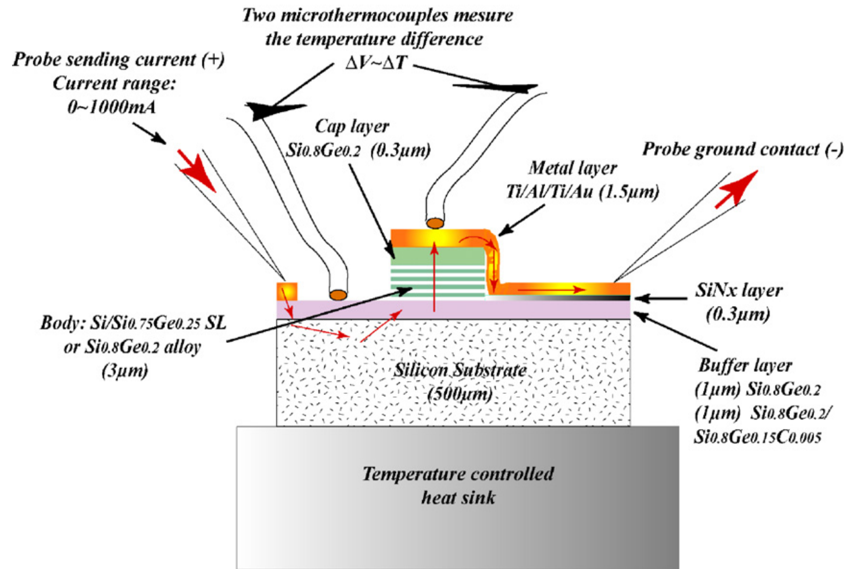


Fig. 6. Schematic diagram of the experimental setup.

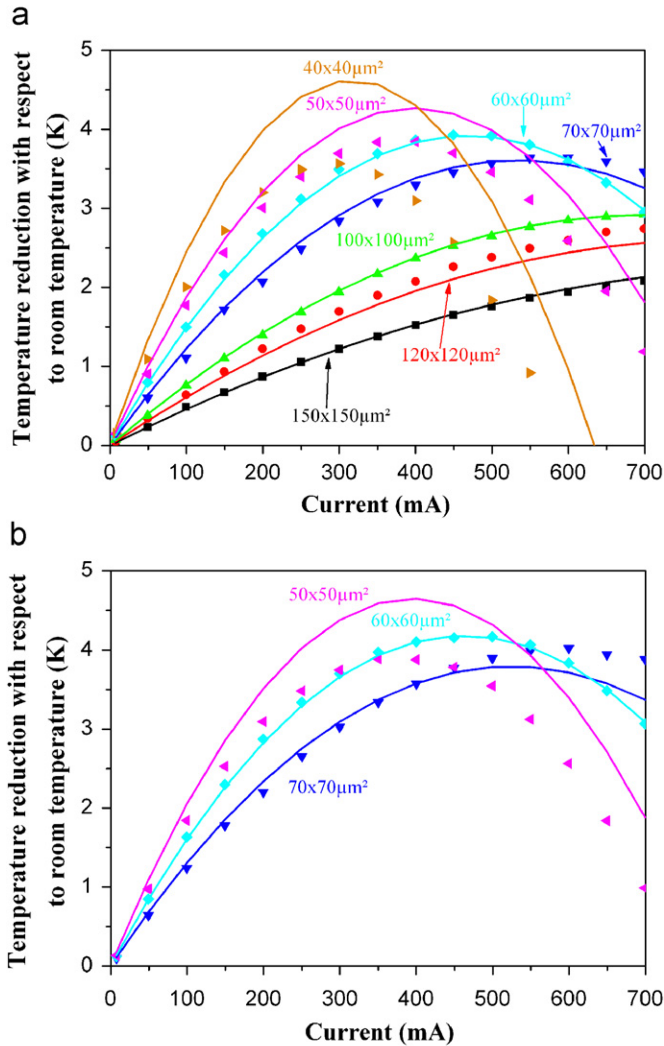


Fig. 7. Measured temperature reduction with respect to room temperature (cooling) on thin film bulk SiGe microrefrigerator (a) and Si/SiGe superlattice microrefrigerator (b) for different device sizes, and their corresponding fits based on thermal quadrupoles method modeling.

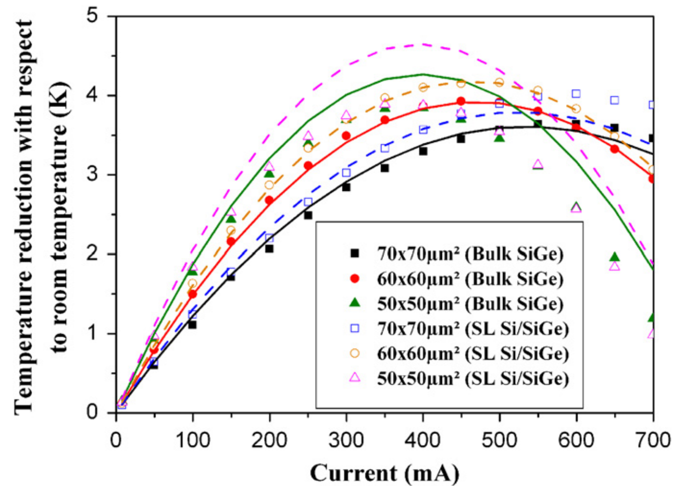


Fig. 8. Comparison of the cooling capacities of bulk SiGe and Si/SiGe superlattices based microrefrigerators for the same sizes. Solid lines are the simulated curves based on thermal qudrupoles method modeling.

trade-off between thermal conductivity and power factor, the overall cooling of the microrefrigerators is similar for the same device sizes. The power factor $\sigma S^2$ in the case of Si/SiGe superlattice is almost 24% higher than that of bulk SiGe alloy.

Eq. (28) gives the simulated temperature variation at the microrefrigerator top surface, $T_{C1}$. We have used this solution in combination with the experimental data of Table 1 to fit the cooling of both bulk SiGe and Si/SiGe superlattice microrefrigerators for all device sizes considered above. The result is shown in Figs. 7 and 8. This model gives a reasonably good fit of the experimental data. For microrefrigerator device size less than $50 \times 50\,\mu m^2$, the fit is not as good. This could be due to the microthermocouple that has the same size and its thermal mass and heat load could affect temperature measurements in the smallest devices.

Table 1
Material parameters for bulk SiGe alloy and Si/SiGe superlattice

| Material | Seebeck coefficient, $S$ (μV/K) | Electrical conductivity, $\sigma$ $(\Omega cm)^{-1}$ | Thermal conductivity, $\beta$ (W/mK) | Power factor, $S^2\sigma$ $(10^{-3}$ W/K m) | Figure-of-merit, $ZT = S^2\sigma T/\beta$ |
|---|---|---|---|---|---|
| $Si_{0.8}Ge_{0.2}$ alloy (micro refrigerator $\Delta T_{max} = 4.0$ K) | 210 | 367 | 5.9 | 1.6 | 0.08 |
| | 210[a] | 375[a] | 6[a] | 1.7[b] | 0.083[b] |
| Superlattice $Si/Si_{0.75}Ge_{0.25}$ (3 nm/12 nm) (micro refrigerator $\Delta T_{max} = 4.2$ K) | 200–220(⊥) | 384[a] | 6.8–8.7(⊥) | 2.28(⊥, estimated) | 0.085(⊥, estimated) |
| | 235[a] 180(‖) | 384(‖) | 8[a] | 1.2(‖) 2.1[b] | 0.080[b] |

Maximum cooling temperature of microrefrigerator devices based on some of the material is also given. Typical microrefrigerator device size is $60 \times 60\,\mu m^2$ and thin film thickness is ~3 μm. (‖) refers to in-plane material properties and (⊥) refers to cross-plane material properties. The estimated cross-plane power factors and ZTs for superlattices are based on the measured maximum cooling of microrefrigerators and the comparison with identical thin film devices based on alloy material.

[a]Refers to values used to get the best fit for all microrefrigerator sizes.

[b]Refers to the calculated power factors and ZTs based on the best fit parameters.

Besides using the developed model to fit the experimental data, we have also considered the optimization of the microrefrigerator's cooling and cooling power density with respect to different geometrical and thermophysical properties. The results demonstrate the existence of an optimum device size and active layer thickness; these optima are strongly dependent of the whole geometry of the microrefrigerator and its physical properties, especially the electrical contact resistance at the interface metal layer/cap layer and the electrical spreading into the substrate [20].

## 6. Conclusion

In this paper, a short comparison between two different silicon-based microrefrigerators was presented. Both Si/SiGe superlattice and bulk SiGe thin film devices have been fabricated and characterized. Experimental data were supported by a detailed theoretical modeling based on TQM. The analysis is used to extract the key factors limiting the performance of the microrefrigerators. Although Si/SiGe superlattice has enhanced electrical properties (larger thermoelectric power factor), the maximum cooling of thin film refrigerators based on SiGe alloys are comparable to that of superlattices. This is due to the fact that the superlattice thermal conductivity is larger than bulk SiGe alloy by about 30%. Microrefrigerators based on bulk SiGe alloys are easier to implement using volume growth techniques such as chemical vapor deposition and they can provide localized cooling in integrated circuit chips. If additional means to reduce superlattice lattice conductivity could be implemented keeping their large thermoelectric power factors, further improvements in the maximum cooling temperature and cooling power density could be achieved.

## Acknowledgments

This work is supported by Interconnect Focus Center, DARPA Heretic and Canon Corp.

## References

[1] D.M. Rowe, Handbook of Thermoelectrics, CRC, Boca Raton, FL, 1995.

[2] D. Vashaee, C. Labounty, X. Fan, G. Zeng, P. Abraham, J.E. Bowers, A. Shakouri, Modeling of thin film P-InGaAs/InGaAsP coolers for integrated optical devices, Proc. SPIE–Int. Soc. Opt. Eng. 4284 (2001) 139–144.

[3] D. Vashaee, J. Christofferson, Y. Zhang, A. Shakouri, G. Zeng, C. Labounty, X. Fan, J.E. Bowers, E.T. Croke, Modeling and optimization of single element bulk SiGe thin film coolers, Micro. Therm. Eng. 9 (2005) 99–118.

[4] Y. Zhang, D. Vashaee, J. Christofferson, G. Zeng, C. LaBounty, J. Piprek, E. T. Croke, A. Shakouri, Heterostructure thin film cooler optimization by 3D Electrothermal simulation, Proceeding of the International Mechanical Engineering Congress and Exposition, Washington, DC, USA, November 16–21, 2003.

[5] D. Maillet, S. André, J.C. Batsale, A. Degiovanni, C. Moyne, Thermal Quadrupoles: Solving the Heat Equation through Integral Transforms, Wiley, New York, 2000.

[6] L. D. Patino-Lopez, S. Grauby, Y. Ezzahri, W. Cleays, S. Dilhaire, Harmonic regime analysis and inverse methods applied to the simultaneous estimation of thermoelectric properties, Proceeding of the 25rd International Conference on Thermoelectrics, Vienna, Austria, August 6–10, 2006.

[7] L. D. Patiño-Lopez, PhD Thesis, ON 2792, University Bordeaux 1, 2004.

[8] Y. Ezzahri, S. Dilhaire, S. Grauby, L. D. Patiño-Lopez, W. Claeys, Y. Zhang, Z. Bian, A. Shakouri, Simulation of Si/SiGe micro-cooler by thermal quadrupoles method, Proceeding of the 24rd International Conference on Thermoelectrics, Clemson, South Carolina, USA, June 19–23, 2005, (pp. 241–245).

[9] Y. Ezzahri, S. Dilhaire, L.D. Patino-Lopez, S. Grauby, W. Claeys, Z. Bian, Y. Zhang, A. Shakouri, Dynamical behavior and cut-off frequency of Si/SiGe microcoolers, Superlattices and Microstructures 41 (2007) 7–16.

[10] Y. Ezzahri, PhD Thesis, ON 3090, University Bordeaux 1, 2005.

[11] J.P. Douglas, Si/SiGe heterostructures: from material and physics to devices and circuits, Semiconductor Science and Technology 19 (2004) 75–108.

[12] A. Shakouri, J.E. Bowers, Heterostructure integrated thermionic coolers, Appl. Phys. Let, 71 (1997) 1234.

[13] A. Shakouri, E.Y. Lee, D.L. Smith, V. Narayanamurti, J.E. Bowers, Thermoelectric effects in submicron heterostructure barriers, Micro. Therm. Eng, 2 (1998) 37–47.

[14] G.D. Mahan, J.O. Sofo, M. Bartkowiak, Multilayer thermionic refrigerator and generator, J. Appl. Phys. 83 (1998) 4683–4689.
[15] A. Shakouri, Thermoelectric, thermionic and thermophotovoltaic energy conversion, Proceeding of the 24rd International Conference on Thermoelectrics, Clemson, SC, USA, June 19–23, 2005, pp. 492–497.
[16] J.M. Ziman, Electrons and Phonons, C. Press, Oxford, 1960.
[17] S. Dilhaire, Y. Ezzahri, S. Grauby, W. Claeys, J. Christofferson, Y. Zhang, A. Shakouri, Thermal and thermomechanical study of micro-refrigerators on a chip based on semiconductor heterostructures, Proceeding of the 23rd International Conference on Thermoelectrics, La Grande Motte, France, 17–21, 2003, pp. 519–523.
[18] P. Wang, A.B. Cohen, B. Yang, G.L. Solbrekken, A. Shakouri, Analytical modeling of silicon thermoelectric microcooler, J. Appl. Phys, 100 (2006) 014501–014513.
[19] S.T. Huxtable, A.R. Abramson, C.L. Tien, A. Majumdar, C. LaBounty, X. Fan, G. Zeng, J.E. Bowers, A. Shakouri, E.T. Croke, Thermal conductivity of Si/SiGe and SiGe/SiGe superlattices, Appl Phys Let 80 (2002) 1737–1739.
[20] Y. Ezzahri, R. Singh, J. Christofferson, Z. Bian, A. Shakouri, Optimization of Si/SiGe microrefrigerators for hybrid solid-state/liquid cooling, Proceeding of InterPACK'07 Conference, in preparation.